Check for updates

Highly selective fluorescent sensor for ammonium ions†

Min Shen,[a] Tingting Pan,*[b] Yonghao Chen,[a] Juewei Ning,[c] Fengyu Su*[d] and Yanqing Tian [ID] *[a]

Ammonium ions (NH_4^+) are one of the important metabolic products and are closely related to human health. Currently, many NH_4^+ detection methods are inevitably disturbed by amino acids, K^+, or other substituted amines (such as trimethylamine). To alleviate this problem, a new sensor was designed in this study, which consisted of the fluorescent indicator **KS**, hydrogel medium D4, and a hydrophobic membrane. In this sensing system, NH_4^+ and NH_3 coexisted in equilibrium; NH_3 could pass through a suitable hydrophobic film and transform into NH_4^+, which complexed with **KS**, resulting in a change of the probe's fluorescence intensity. By adjusting the internal composition of the sensing matrix, an excellent NH_4^+ sensor **NS-1** was obtained; it demonstrated effective detection of NH_4^+ in the range 0.3–15.6 mM with a limit of detection (LOD) of 258 μM, and it was not disturbed by K^+ or other substituting amines.

1. Introduction

Ammonia plays an important role in the human body and is considered an important biomarker. In aquatic environments, ammonium exists mainly as ammonium ions (NH_4^+). NH_4^+ is a common cellular metabolite, produced by the degradation of glutamine. Recently, different views have emerged regarding the role of NH_4^+ in cells. One hypothesis states that NH_4^+ is a metabolic product that inhibits cell growth.[1] As far as ammonia is concerned, 10 mM is toxic to all mammalian cells.[2] Another hypothesis states that a moderate amount of NH_4^+ can promote tumor growth and support biomass production.[3,4] Therefore, further research on the metabolism mechanism in cells is necessary. On the other hand, adults produce about 1000 mmol of ammonia per day, some of which can be reused in biosynthesis, while the rest is useless and even neurotoxic.[5] For example, the approximate level of plasma NH_4^+ is 10–50 μmol L^{-1},[6] and excessive NH_4^+ in the blood can inhibit the normal metabolism of the brain, thus causing diseases. Hepatic encephalopathy is a disease caused by abnormal blood ammonia metabolism.[7,8] The relationship between NH_4^+ and health can also be found in many other body fluids, such as urine,[9,10] sweat,[11,12] and saliva;[13,14] the approximate levels of salivary NH_4^+ and sweat NH_4^+ are 0.85–5.5 mmol L^{-1} (ref. 15) and 0.5–8 mmol L^{-1},[16] respectively. In short, NH_4^+ is an important metabolic marker closely related to human health; therefore, it is of great importance to prepare appropriate tools for NH_4^+ detection.

The ion-selective electrode (ISE) is a classical sensor for the detection of NH_4^+.[17,18] It has the advantage of being small in size and easy to operate. Nonactin, the most commonly used ionophore in ISE, binds well to NH_4^+.[19,20] However, it can also bind K^+.[21] Therefore, the presence of K^+ can cause interference with the test results. Another commonly available commercial ammonia electrode is the ammonia gas sensitive electrode,[22,23] which uses a pH glass electrode as the indicator electrode; the NH_4^+ in the sample is converted to NH_3 and diffuses through the semi-permeable membrane, causing a change of pH. The device is simple to operate; however, samples need to be pre-treated and the analysis result is highly susceptible to interference by other volatile amines such as trimethylamine (TMA).

In recent years, several optical sensors have been gradually developed for NH_4^+ detection. Colorimetric tests based on Nessler,[24,25] and Berthelot[26–28] reactions are two of the more common methods used for NH_4^+ detection. They are

[a] *Department of Materials Science and Engineering, Southern University of Science and Technology, Xili, Nanshan District, Shenzhen 518055, China. E-mail: tianyq@sustech.edu.cn*

[b] *Department of Pediatric Neurology, Shenzhen Children's Hospital, 7019 Yitian Road, Shenzhen 518038, China. E-mail: pantingting_2022@163.com*

[c] *Ganjiang Innovation Academy, Chinese Academy of Sciences, Ganzhou 341119, China*

[d] *Academy of Advanced Interdisciplinary Studies, Southern University of Science and Technology, Xili, Nanshan District, Shenzhen, 518055, China. E-mail: fysu@sustech.edu.cn*

technically mature, but the detection process is cumbersome and involves toxic reagents, such as phenol, hypochlorite, and mercury. In addition, their detection results are easily interfered with by colored compounds. Another common optical ammonia sensor is designed based on a pH indicator, where ammonia reacts with the pH indicator, and the pH indicator is then deprotonated, resulting in changes in absorption and fluorescence. The drawback of this method is that it is susceptible to pH and other volatile amines.[29,30] To solve this pH interference problem, Flood et al. proposed a new method for ion assay by ion-pair formation. Stromberg[31] introduced the NH_4^+ selective ionophore nonactin for the NH_4^+ assay; Jonah et al.[32] used pyrazole to accomplish this, they have a common disadvantage, which is the interference of potassium ions. Since the ionic radii of NH_4^+ (286 pm) and K^+ (266 pm) are similar, it is difficult to distinguish between these two cations, which poses a challenge for designing the NH_4^+ sensor without K^+ interference. In summary, the detection of NH_4^+ is challenging due to the interference of pH and K^+, a sensor with high selectivity for NH_4^+ is necessary.[33]

To alleviate this problem, a new sensor **NS** was designed, which consisted of the triazacryptand (TAC)-containing fluorescent indicator **KS**, hydrogel medium D4, and hydrophobic membrane PTFE (Scheme 1). In this sensing system, NH_4^+ and NH_3 coexisted in equilibrium, and NH_3 passed through a proton/ion barrier using polytetrafluoroethylene (PTFE) membrane and is converted to NH_4^+ in the sensing matrix. The formed NH_4^+ can form a complex with **KS**, leading to an increase in fluorescence. Contrary to the common optical NH_4^+ sensor, the use of TAC reduces the interference from other substituted amines, and the use of PTFE membrane shields some of the other potential interfering ions such as K^+.

2. Experimental section

2.1. Materials

L-Arginine, L-histidine, L-isoleucine, L-leucine, L-lysine, L-valine, bis(2-hydroxyethyl)imino-tris(hydroxymethyl)methane (Bis-Tris), and tris(hydroxymethyl)aminoethane (Tris) were purchased from Bide Pharmatech Co., Ltd. (Shanghai, China); 4-(2-hydroxyethyl)-1-piperazineethanesulfonic acid (HEPES), potassium chloride (KCl), and ammonium chloride (NH_4Cl) were purchased from Aladdin (Shanghai, China); polyurethane hydrogel (D4) was obtained from Heowns Biochem Technologies, LLC. (Tianjin, China); DMEM medium was purchased from Baishengyue Biotechnology Co., Ltd. (Shanghai, China); L-glutamine solution was purchased from Melone Pharmaceutical Co., Ltd. (Dalian, China). PTFE membrane was purchased from Tian Xiang Industry Co., Ltd. (Shenzhen, China).

### 2.2. Materials characterization

A spectrofluorophotometer (RF-6000, PerkinElmer, Japan) and multi-mode microplate reader (Cytation3, BioTek, Winooski, VT, USA) were used.

2.3. Sensor preparation and characterization

The indicator **KS** was synthesized according to our previous report,[34] a PTFE membrane was employed as a proton/ion barrier, and a drop-coating method was employed to prepare the sensors. Two types of sensor films were prepared for comparison.

Sensor NS0 without PTFE membrane. NS0 consisted of a substrate, a fluorescent indicator **KS**, and a hydrogel medium. Hydrogel D4 (100 mg) and **KS** (0.1 mg) were dissolved in 1 ml of ethanol. Then, 20 μl of the above solution was dropped onto the quartz glass as the sensor substrate with an 8 mm circular pattern. Finally, the film was characterized using a spectrofluorophotometer after drying at room temperature.

Sensors NS with PTFE membrane. **NS** contains the fluorescent indicator **KS**, hydrogel medium D4, and PTFE membrane. The hydrogel D4 (100 mg) was dissolved in 1 ml of the mixed solvent (EtOH : buffer = 9 : 1). The buffer was made from Bis-Tris and HCl, with different buffer capacities and pH (Table 1). The indicator **KS** (0.1 mg) was then added into the mixtures of the D4 hydrogel and buffer
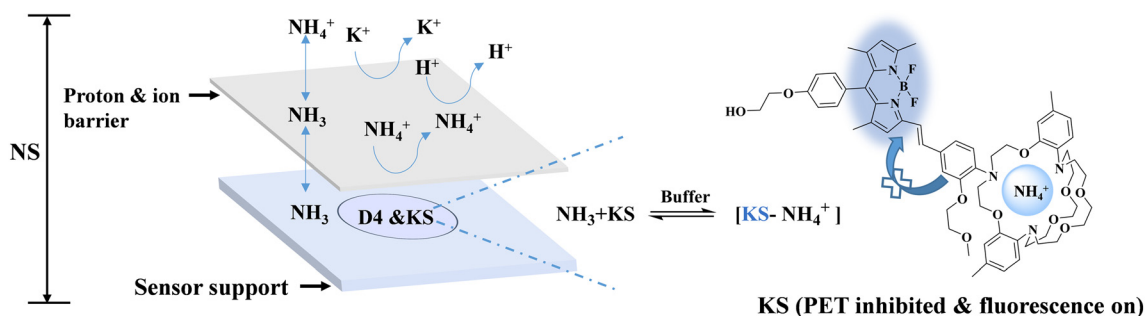
Scheme 1 Schematic diagram of **NS** for NH_4^+ detection. NH_4^+ and NH_3 coexist in equilibrium in the solution. NH_3 can pass through the proton/ion barrier and is converted to NH_4^+, which forms a complex with the TAC–containing fluorescent probe (**KS**) in the buffer between the barrier and substrate, leading to an increase in fluorescence in the sensing matrix. Because of the proton/ion barrier, NH_4^+ or other ions in the solution were blocked, thus achieving high selectivity (here, **NS** includes **NS-1**, **NS-2**, **NS-3**, and **NS-4**, which differ mainly in the internal buffers).

Table 1 Compositions of buffers corresponding to different sensors

Sensor	Ingredient	Concentration	pH value	FEF
NS-1	Bis-Tris-HCl	1000 mM	6.5	11.68
NS-2	Bis-Tris-HCl	100 mM	6.5	7.92
NS-3	Bis-Tris-HCl	1000 mM	7	6.82
NS-4	Bis-Tris-HCl	NO	NO	1.28

FEF: fluorescence enhancement factor (I/I_0 at 62.4 mM).

to yield a stock solution. 20 μl of the stock solution was dropped in the circular area of the substrate. Herein, a 12- well plate with an 8-mm circular pattern was used as the substrate. Finally, the PTFE membrane was glued on top by the UV curing adhesive to prevent the entry of ions and protons from the analytes. Finally, the sensing properties of the **NS** were characterized using a multi-mode microplate reader.

The LOD calculation. The LOD was calculated using the following equations:
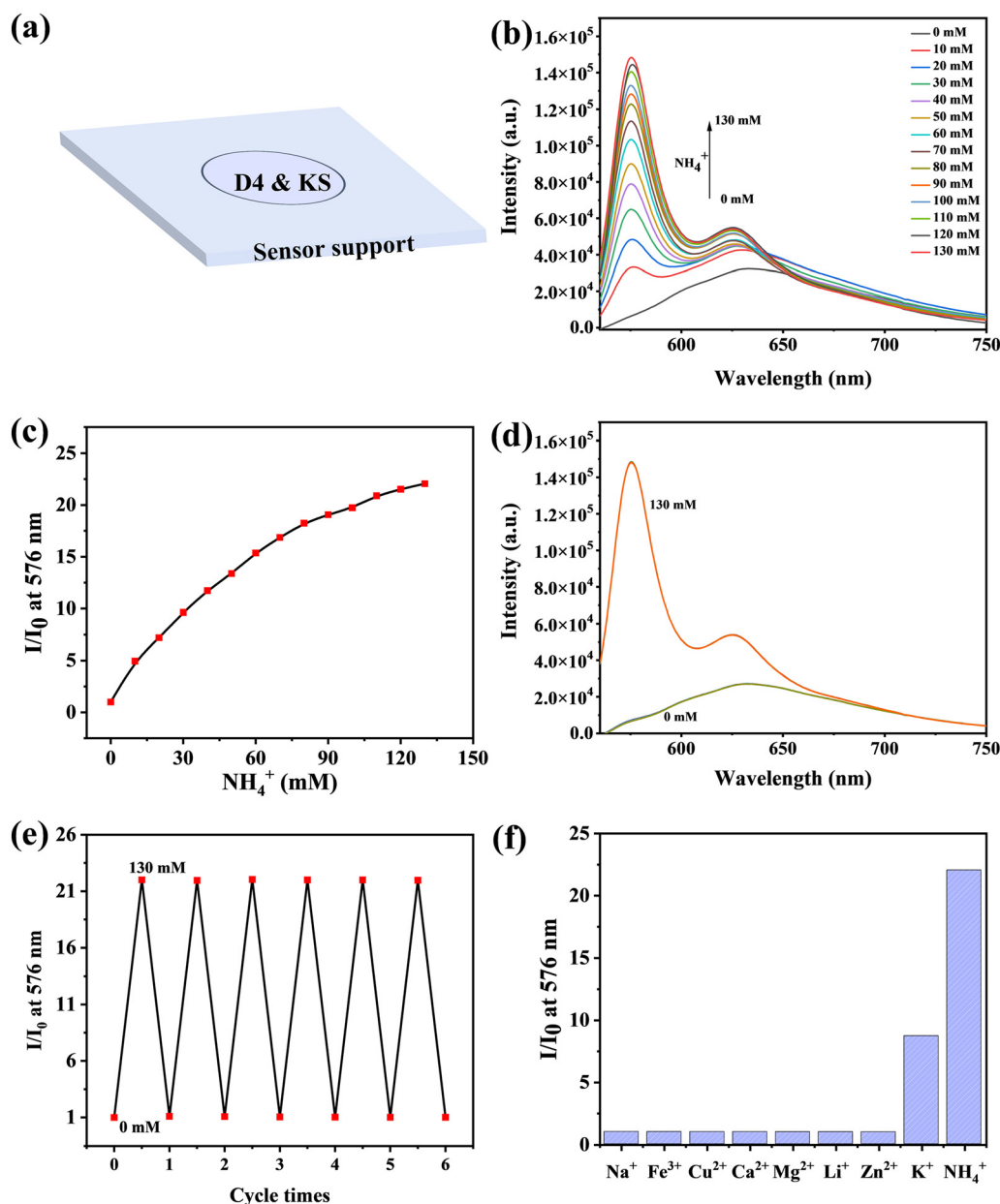
$$y = \frac{3\delta}{k}$$

Fig. 1 (a) Schematic of sensor **NS0** without the PTFE membrane, (b) the emission spectrum of **NS0** during NH_4^+ titration, (c) variation of emission intensity at the main emission peak (576 nm) upon NH_4^+ addition, (d) the emission spectra of **NS0** during NH_4^+-free and NH_4^+-rich cycles, (e) cyclic stability of **NS0**, (f) selectivity of **NS0** (Na^+ (NaCl, 150 mM), Fe^{3+} ($FeCl_3$, 50 μM), Cu^{2+} ($CuCl_2$, 50 μM), Ca^{2+} ($CaCl_2$, 2 mM), Mg^{2+} ($MgCl_2$, 2 mM), Li^+ (LiCl, 150 mM), Zn^{2+} ($ZnSO_4$, 2 mM), K^+ (KCl, 20 mM), and NH_4^+ (NH_4Cl, 130 mM)).

where σ is the standard deviation of the blank sample and k is the slope of the calibration curve.

Monitoring of the breakdown of glutamine. First, glutamine was added to DMEM to prepare a solution with glutamine, and then, the solution was stored at different temperatures (4 °C, room temperature, and 37 °C) for different periods of time (0, 3, 6, 9, 12, days). Finally, **NS-1** was employed to detect the NH_4^+ produced by the breakdown of glutamine.

2.4. Design of the sensor NS

(1) It has been known that NH_4^+ and NH_3 in the solution are coexisting.[35] Specifically, NH_4^+ in an aqueous sample can dissociate into NH_3 with dynamic equilibrium. This coexistence is well described by a classical formula called the Henderson–Hasselbalch equation (eqn (1)).[35]

$$pH = pK_a - \log([NH_4^+]/NH_3) \tag{1}$$

However, NH_4^+ and NH_3 are two existential forms of ammonia with different properties. NH_3 can pass through a suitable hydrophobic film, whereas NH_4^+ cannot.

(2) When the layer of the hydrophobic and gas permeable PTFE film was placed on the top of the sensor's detection area, the PTFE film could act as a barrier for ions and protons. Thus, K^+ was isolated outside the PTFE membrane and could not contact the probe **KS** in the detection area. Therefore, the interference of K^+ was skillfully eliminated, whereas NH_3 in the analytes could pass through the PTFE membrane and combine with the proton of the buffer in the D4 hydrogel to form new NH_4^+. The generated NH_4^+ complexes with the probe **KS**, showing similar fluorescence responses similar to **NS0**.

3. Results and discussion

3.1. Responses of NS0 to NH_4^+

As shown in Fig. 1a, **NS0** comprises a substrate, fluorescent indicator **KS**, and hydrogel medium. For sensing, it is important to choose an appropriate polymer matrix for the indicator. Herein the commercial D4, consisting of hydrophobic and hydrophilic sections with a water-absorbing capability of 50%,[36] was selected.

The responsiveness of **NS0** to NH_4^+ was then investigated. With the addition of NH_4^+, the fluorescence of **NS0** increased gradually (Fig. 1b). The main fluorescence emission peak was at 576 nm, and the fluorescence enhancement factor could reach 22 upon adding 130 mM of NH_4^+ (I/I_0 at 130 mM), indicating the high sensitivity (Fig. 1c). Subsequently, the cycle stability of **NS0** was tested using NH_4^+-free and NH_4^+-rich cycles. The detection ability of the sensor basically did not change, showing good cycle stability (Fig. 1d and e). In addition, the selectivity of the sensor was investigated. The results showed that if **NS0** was used directly as the NH_4^+ sensor, K^+ would cause serious interference (Fig. 1f). Most

likely, this is due to the fact that both K^+ and NH_4^+ are cations, and the ionic radii of K^+ (266 pm) is similar to that of NH_4^+ (286 pm), which matches the size of the cavity of the cryptand (TAC).[32] Therefore, **NS0** needs to be modified to exclude K^+ interference to become an excellent NH_4^+ sensor.

This fluorescence enhancement can be explained by the mechanism of photo-induced electron transfer (PET).[37,38] Before NH_4^+ binds to **KS**, the lone pair of electrons of nitrogen atoms on TAC quenched the fluorophore emission by PET. When NH_4^+ binds to the probe molecule, PET is suppressed, and fluorescence is enhanced (Scheme S1†).

3.2. Response of NS to NH_4^+

In order to alleviate the K^+ interferences on **NS0**, as mentioned above, a new sensor **NS** was designed (Scheme 1) by adding a hydrophobic membrane on the top.

3.2.1. Optimization of the sensor NS. Similar to **NS0**, the fluorescent indicator **KS** is responsible for the NH_4^+ response, and hydrogel D4 is used to carry the fluorescent probe. While the PTFE membrane is the barrier for protons and ions. In addition to the above three materials, there is another component that deserves special mention, the buffer inside the D4 hydrogel. The buffer acts as a proton reservoir to help convert NH_3 to NH_4^+, which may have a great impact on the sensing performance. Therefore, four sensors (**NS-1**, **NS-2**, **NS-3**, and **NS-4**) containing buffers with different buffer capacities and pH values were prepared to explore the impact of buffers on the sensors performance. The compositions of buffers used for the preparation of different sensors are listed in Table 1.

Since these four sensors' compositions are similar, they have similar emission spectra. Representative fluorescence spectra of **NS-1** are shown in Fig. 2a, and the remaining ones are shown in Fig. S1.† The main fluorescence emission peak was located at 576 nm, and the fluorescence intensity increased with increasing NH_4^+ concentrations.

However, they differed in their ability to respond to NH_4^+, which was attributed to the differences in buffer capacities and pH values. Fig. 2b shows the effects of the buffer capacity on the sensing performance. Compared with **NS-2** and **NS-4**, **NS-1** had a wider detection range and higher sensitivity when detecting NH_4^+, because it had a strong buffer capacity (1000 mM) in the sensing region, which could provide more protons for NH_3 to convert to NH_4^+. The sensitivity of the sensor gradually increased as the pH of the buffer in the detection area decreased (Fig. 2c). This is because the buffers with lower pH are more likely to supply NH_3 with more protons. The sensor without buffer (**NS-4**) in the sensing area was set as a control, which was basically unresponsive to NH_4^+.

Theoretically, the smaller the pH value of the buffer in the sensing region, the higher the sensitivity of the sensor. However, the pH value cannot be too small, which is limited by the nature of probe **KS** itself. This is because nitrogen atoms on TAC would be protonated when pH is too low, thus
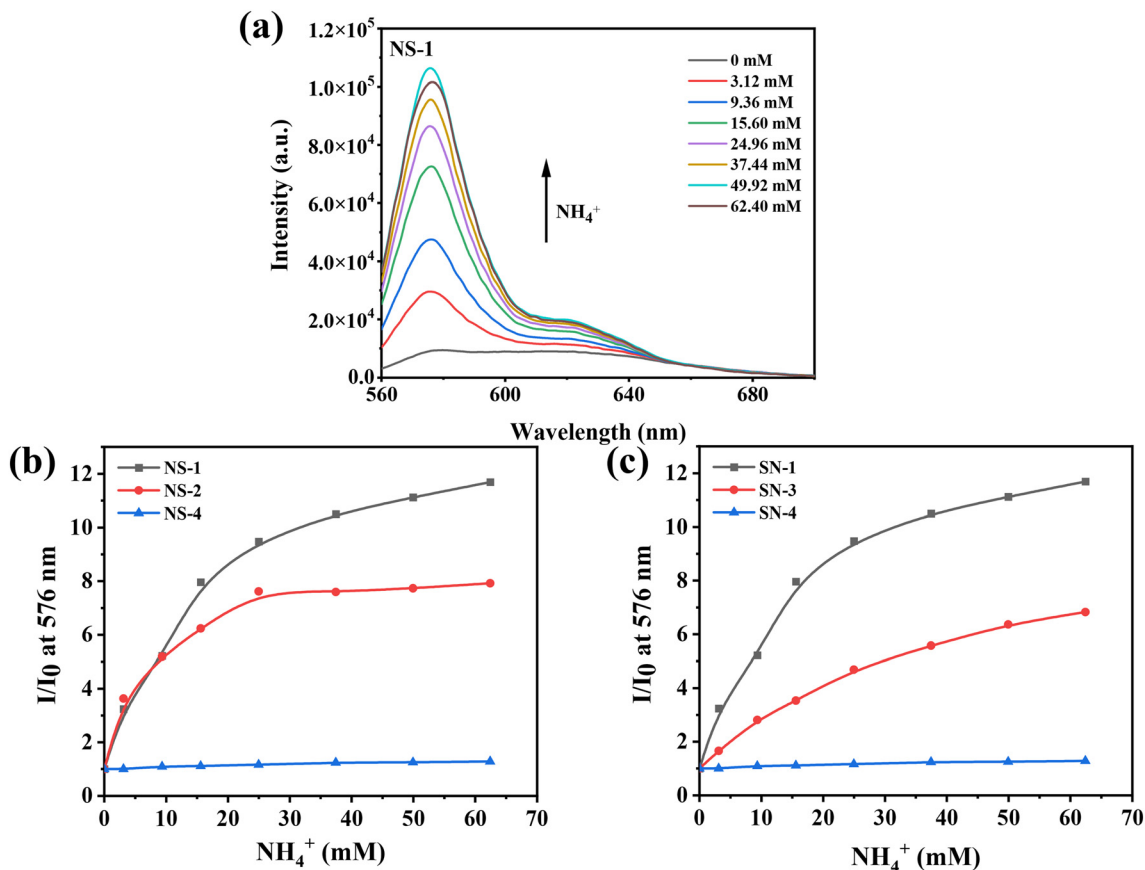
Fig. 2 Effects of buffer in the detection area on the sensor performance. (a) Emission spectra of the sensor **NS-1** with buffer (1000 mM, pH = 6.5) at different NH_4^+ concentrations. (b) Plots of the fluorescence intensity ratio (I/I_0) at 576 nm against NH_4^+ of sensors with different buffer capacities. (c) Plots of the fluorescence intensity ratio (I/I_0) at 576 nm against NH_4^+ of sensors containing buffers with different pH values.

weakening its photoinduced electron transfer effect and enhancing fluorescence. As shown in Fig. S2a and b,† when the pH value was less than 6, the fluorescence increased gradually with the decrease of the pH value. Under these conditions, if other substituted amines such as TMA enter the protonated nitrogen would be deprotonated and the

fluorescence would weaken, thus causing interference (Scheme S2†). Here, TMA was used as a substituted amine model for the interference exploration, and the result is shown in Fig. S2c;† the fluorescence intensity of this sensor (pH value of buffer was 6) was reduced with the addition of TMA, indicating that buffers with pH less than 6 were not
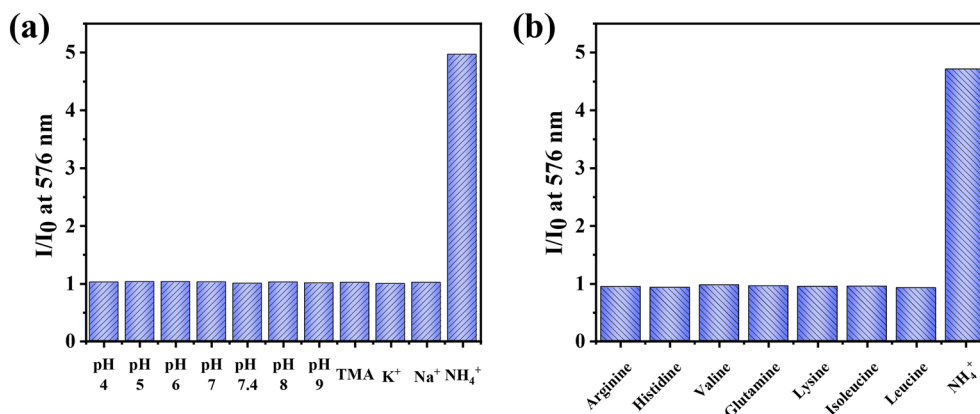

Fig. 3 (a) Potential interference from pH (pH = 4–9), ions (20 mM K^+, 20 mM Na^+), or TMA (2 mg L^{-1}). (b) Potential interference from common amino acids in the culture medium. Arginine (84 mg L^{-1}), histidine (42 mg L^{-1}), valine (94 mg L^{-1}), glutamine (584 mg L^{-1}), lysine (146 mg L^{-1}), isoleucine (105 mg L^{-1}), L-leucine (105 mg L^{-1}), and NH_4^+ (8.5 mM).

good choices. When the pH value ranged from 6 to 8, the fluorescence intensity was not affected by the pH value. Therefore, we chose 6.5 as the appropriate pH value, which ensured that not only the nitrogen atoms on the TAC were not protonated, and also that the sensor had a high sensitivity.

After the above exploration, sensor **NS-1** with buffer (Bis-Tris/HCl, 1000 mM, pH = 6.5) was used in subsequent experiments; it demonstrated an effective detection of NH_4^+ in the range of 0.3–15.6 mM with the limit of detection (LOD) of 258 μM (Fig. S3†).

3.2.2. Selectivity and stability. As mentioned above, when **NS0** was used for NH_4^+ detection, the results would be disturbed by K^+. Therefore, we introduced the PTFE membrane that acted as a barrier for protons and ions to avoid such interferences. Here, the shielding effect of the PTFE film was verified. As shown in Fig. 3a, the sensitivity was not affected either by the pH of the detected solutions from 4 to 9, or by K^+, and Na^+ in the solutions, which was attributed to the barrier PTFE membrane. In addition, the absence of interference from the substituted amines was verified using the TMA model.

In addition to the study of the potential interferences from protons and ions, we also investigated whether the common amino acids in the culture medium could cause interference on sensing. As shown in Fig. 3b, the effect of amino acids on the detection was negligible. Therefore, it is superior to the commercially available Amplite colorimetric ammonia quantification kit (AAT Bioquest), wherein the results are interfered by a variety of amino acids.[39]

Furthermore, the cyclic stability of the sensor was tested using NH_4^+-free and NH_4^+-rich cycles. As shown in Fig. S4a,† the detection efficiency of **NS-1** did not significantly decrease during the four cycles, demonstrating its potential for reuse. The stability of the sensor was characterized by irradiation with a high-energy xenon lamp (5 W), and the specific program was set as: runtime 10 min, interval 5 seconds, 121 reads. The results are shown in Fig. S4b† with only a weak decrease in the fluorescence intensity, demonstrating its excellent stability.
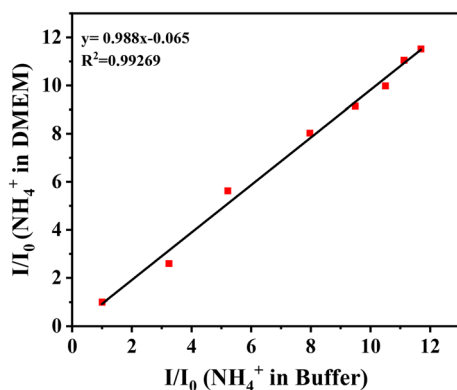

Fig. 4 Detection of NH_4^+ in DMEM.

4. Application

4.1. Detection of NH_4^+ in DMEM

In order to demonstrate the practical utility, **NS-1** was used to determine the concentration of NH_4^+ in samples with complex compositions. NH_4^+ was artificially added to the samples and detected using **NS-1**. As shown in Fig. 4, even in the DMEM, with complex compositions including sugars, amino acids, and salts, **NS-1** worked as well as it did in the HEPES buffer. There is a good correlation between them, and the slope was close to 1, indicating that **NS-1** has the potential for the detection of NH_4^+ in complex environments.

4.2. Monitoring of the breakdown of glutamine

Glutamine is a vital essential amino acid in mammalian growth, which not only serves as the donor of the nitrogen source and carbon source but also provides energy for cell metabolism.[40] Glutamine could be hydrolyzed to produce ammonia. The hydrolysis process is mainly carried out in two ways: one is chemical degradation to produce ammonia and pyrrolidone carboxylic acid; the other is hydrolyzed by glutaminase to produce ammonia and glutamic acid. Here, **NS-1** was tentatively used to detect the breakdown of glutamine. As shown in Fig. 5a, the fluorescence intensity increased gradually with the increase of time, indicating an increase in NH_4^+ levels. The increase was more obvious at room temperature than at 4 °C and the fastest at 37 °C, indicating that the degradation process was accelerated with the increase of the temperature. According to the relationship between changes in the fluorescence intensity and NH_4^+ concentration, the fluorescence intensity changes were converted into NH_4^+ concentration (Fig. 5b).

4.3. Patterning on a flexible substrate

In recent years, bio-diagnostic sensors working in the form of wearable flexible devices have gradually attracted research interest and are of great importance in the monitoring of human health. More and more research teams are reporting wearable sensor devices based on tattoos or fabric to achieve real-time monitoring of various electrolytes and metabolites.[41–44] It would be of great interest if the NH_4^+ sensing system in this study could be presented in the form of a wearable flexible device that could monitor the health information of the body through fluorescent signals. Therefore, we examined the molding capability of the system on the flexible substrate. As shown in Fig. S5,† it could be well shaped on the PET film, a common flexible substrate. Fig. S5a† shows the pattern under daylight lamp and ultraviolet lamp in the absence of NH_4^+; after contact with NH_4^+, the fluorescence was significantly enhanced under the UV lamp (Fig. S5b†). It could be presented in other patterns (Fig. S5c†). Moreover, it could be bent, and twisted, showing significant potential for flexible wearable NH_4^+ detection devices (Fig. S5d†).
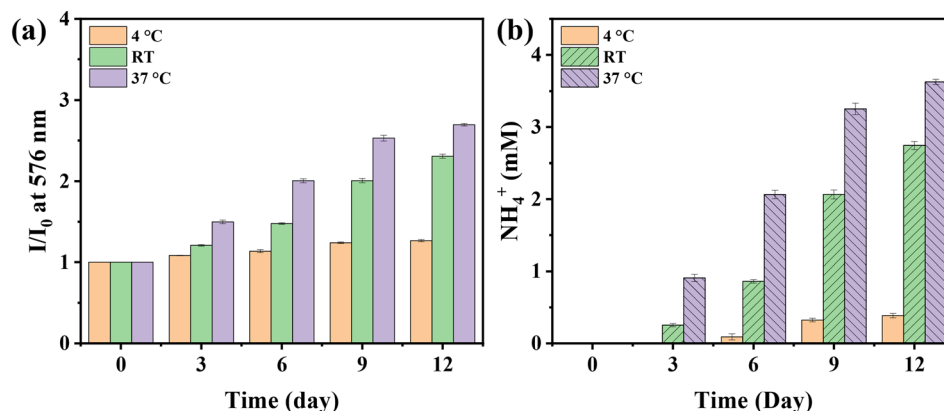
Fig. 5 Monitoring the breakdown of glutamine stored under different conditions. (a) Changes in the fluorescence intensity caused by glutamine decomposition. (b) NH_4^+ released by the breakdown of glutamine.

5. Conclusion

In summary, a novel idea was introduced to design an NH_4^+ sensor by employing the TAC-based fluorescent probe and PTFE membrane. Unlike common NH_4^+ probes, this type of sensor is not designed based on pH indicators and is not disturbed by other substituted amines. Ingeniously, the potential ionic interference was also eliminated by introducing the PTFE membrane. Four groups of sensors (**NS-1**, **NS-2**, **NS-3**, and **NS-4**) containing buffers of different buffering capacities and pH values were prepared to optimize the sensor formula with high sensitivity. After the comparison, **NS-1** is considered as the best candidate, because it exhibited high sensitivity, selectivity, and excellent cyclic stability. In addition, **NS-1** was used to detect NH_4^+ levels in DMEM and successfully monitored the breakdown of glutamine. It can also be molded on a flexible substrate, showing great potential in flexible wearable devices for NH_4^+ detection.

Author contributions

Min Shen: investigation, data curation, and writing of the manuscript; Tingting Pan: funding acquisition and revision of the manuscript; Yonghao Chen: data curation and revision the manuscript; Juewei Ning: guide to synthesize probe KS; Fengyu Su: conceptualization and funding acquisition; Yanqing Tian: conceptualization, funding acquisition, and project administration.

Conflicts of interest

The authors declare that they have no known competing financial interests or personal relationships that could have appeared to influence the work reported in this paper.

Acknowledgements

References

1 I. S. P. Savizi, N. Maghsoudi, E. Motamedian, N. E. Lewis and S. A. Shojaosadati, *Appl. Microbiol. Biotechnol.*, 2022, **106**, 1113–1126.

2 P. J. Price, *In Vitro Cell. Dev. Biol.: Anim.*, 2017, **53**, 673–681.

3 L. Li, Y. Mao, L. Zhao, L. Li, J. Wu, M. Zhao, W. Du, L. Yu and P. Jiang, *Nature*, 2019, **567**, 253–256.

4 J. B. Spinelli, H. Yoon, A. E. Ringel, S. Jeanfavre, C. B. Clish and M. C. Haigis, *Science*, 2017, **358**, 941–946.

5 S. Matoori and J. C. Leroux, *Adv. Drug Delivery Rev.*, 2015, **90**, 55–68.

6 R. J. Barsotti, *J. Pediatr.*, 2001, **138**, S11–S20.

7 J. Yang, M. Yin, Y. Hou, H. Li, Y. Guo, H. Yu, K. Zhang, C. Zhang, L. Jia, F. Zhang, X. Li, H. Bian and Z. Li, *Cell Biosci.*, 2022, **12**, 16–31.

8 V. Liere, G. Sandhu and S. DeMorrow, *F1000Research*, 2017, **6**, 1637–1650.

9 M. Vallet, M. Metzger, J. P. Haymann, M. Flamant, C. Gauci, E. Thervet, J. J. Boffa, F. Vrtovsnik, M. Froissart, B. Stengel, P. Houillier and G. NephroTest Cohort Study, *Kidney Int.*, 2015, **88**, 137–145.

10 K. L. Raphael, *Am. J. Kidney Dis.*, 2019, **74**, 263–275.

11 T. Guinovart, A. J. Bandodkar, J. R. Windmiller, F. J. Andrade and J. Wang, *Analyst*, 2013, **138**, 7031–7039.

12 I. Alvear-Ordenes, D. Garcia-Lopez, J. A. De Paz and J. Gonzalez-Gallego, *Int. J. Sports Med.*, 2005, **26**, 632–637.

13 Y. Thepchuay, C. F. Costa, R. B. Mesquita, B. Sampaio-Maia, D. Nacapricha and A. O. Rangel, *Bioanalysis*, 2020, **12**, 455–465.

14 S. Bevc, E. Mohorko, M. Kolar, P. Brglez, A. Holobar, D. Kniepeiss, M. Podbregar, N. Piko, N. Hojs, M. Knehtl, R. Ekart and R. Hojs, *Clin. Nephrol.*, 2017, **88**, 14–17.

15 J. R. Huizenga, A. Vissink, E. J. Kuipers and C. H. Gips, *Clin. Oral Investig.*, 1999, **3**, 84–87.

16 K. Sato, The Physiology, Pharmacology, and Biochemistry of the Eccrine Sweat Gland, in *Reviews of Physiology, Biochemistry and Pharmacology*, ed. R. H. Adrian, E. Helmreich, H. Holzer, R. Jung, K. Kramer, O. Krayer, R. J. Linden, F. Lynen, P. A. Miescher, J. Piiper, H. Rasmussen, A. E. Renold, U. Trendelenburg, K. Ullrich, W. Vogt and A. Weber, Springer-Verlag Berlin Heidelberg, Berlin, 1977, pp. 51-131.

17 M. Cuartero and G. A. Crespo, *Curr. Opin. Electrochem.*, 2018, **10**, 98–106.

18 R. Athavale, I. Kokorite, C. Dinkel, E. Bakker, B. Wehrli, G. A. Crespo and A. Brand, *Anal. Chem.*, 2015, **87**, 11990–11997.

19 L. A. R. Pioda, H. A. Wachter, R. E. Dohner and W. Simon, *Helv. Chim. Acta*, 1967, **50**, 1373–1376.

20 J. Gallardo-Gonzalez, A. Baraket, S. Boudjaoui, T. Metzner, F. Hauser, T. Rossler, S. Krause, N. Zine, A. Streklas, A. Alcacer, J. Bausells and A. Errachid, *Sci. Total Environ.*, 2019, **653**, 1223–1230.

21 H. A. N. John, S. Benco and W. G. McGimpsey, *Anal. Chem.*, 2003, **75**, 152–156.

22 L. R. McKenzie and P. N. W. Young, *Analyst*, 1975, **100**, 620–628.

23 C. Henriquez, B. Horstkotte and V. Cerda, *Talanta*, 2014, **118**, 186–194.

24 L. N. Demutskaya and I. E. Kalinichenko, *J. Water Chem. Technol.*, 2010, **32**, 90–94.

25 A. Skok, Y. Bazel and A. Vishnikin, *Chem. Pap.*, 2023, DOI: 10.1007/s11696-023-02903-3.

26 K. N. Lin, P. C. Li, Q. L. Wu, S. C. Feng, J. Ma and D. X. Yuan, *Microchem. J.*, 2018, **138**, 519–525.

27 H. Yu, G. Zhang, Y. Cai and F. Dong, *Anal. Bioanal. Chem.*, 2021, **413**, 5695–5702.

28 Y. B. Cho, S. H. Jeong, H. Chun and Y. S. Kim, *Sens. Actuators, B*, 2018, **256**, 167–175.

29 G. Musile, R. Gottardo, C. Palacio, K. Shestakova, D. Raniero, E. F. De Palo and F. Tagliaro, *Forensic Sci. Int.*, 2019, **295**, 150–156.

30 B. M. Jayawardane, I. D. McKelvie and S. D. Kolev, *Anal. Chem.*, 2015, **87**, 4621–4626.

31 N. Stromberg and S. Hulth, *Anal. Chim. Acta*, 2001, **443**, 215–225.

32 T. M. Jonah, L. Mathivathanan, A. N. Morozov, A. M. Mebel, R. G. Raptis and K. Kavallieratos, *New J. Chem.*, 2017, **41**, 14835–14838.

33 A. Rahman, N. H. Kwon, M. S. Won, M. H. Hyun and Y. B. Shim, *Anal. Chem.*, 2004, **76**, 3660–3665.

34 H. T. Liu, J. W. Ning, G. J. Song, X. Z. Sun, F. Y. Su, P. F. Li and Y. Q. Tian, *Spectrochim. Acta, Part A*, 2020, **232**, 118155–118160.

35 H. N. Po and N. M. Senozan, *J. Chem. Educ.*, 2001, **78**, 1499–1503.

36 Z. Cao, Q. Zhu, R. C. Aller and J. Y. Aller, *Mar. Chem.*, 2011, **123**, 23–31.

37 M. Shen, T. Pan, J. Ning, F. Sun, M. Deng, J. Liao, F. Su and Y. Tian, *Spectrochim. Acta, Part A*, 2022, **279**, 121435–121444.

38 T. Pan, M. Shen, J. Shi, J. Ning, F. Su, J. Liao and Y. Tian, *Sens. Actuators, B*, 2021, **345**, 130450–130459.

39 E. Dervisevic, N. H. Voelcker, G. Risbridger, K. L. Tuck and V. J. Cadarso, *ACS Sens.*, 2020, **5**, 2523–2529.

40 K. Vanhove, E. Derveaux, G. J. Graulus, L. Mesotten, M. Thomeer, J. P. Noben, W. Guedens and P. Adriaensens, *Int. J. Mol. Sci.*, 2019, **20**, 252–268.

41 V. F. Curto, C. Fay, S. Coyle, R. Byrne, C. O'Toole, C. Barry, S. Hughes, N. Moyna, D. Diamond and F. Benito-Lopez, *Sens. Actuators, B*, 2012, **171**, 1327–1334.

42 H. Lee, T. K. Choi, Y. B. Lee, H. R. Cho, R. Ghaffari, L. Wang, H. J. Choi, T. D. Chung, N. S. Lu, T. Hyeon, S. H. Choi and D. H. Kim, *Nat. Nanotechnol.*, 2016, **11**, 566–574.

43 M. M. Hossain, B. M. Li, B. Sennik, J. S. Jur and P. D. Bradford, *npj Flexible Electron.*, 2022, **6**, 97–103.

44 S. Zhang, A. Chhetry, M. A. Zahed, S. Sharma, C. Park, S. Yoon and J. Y. Park, *npj Flexible Electron.*, 2022, **6**, 11–22.